Initial Stages of the HCl-Induced High-Temperature Corrosion of Alloy 310

N. Folkeson,[z] L.-G. Johansson,* and J.-E. Svensson*

*Department of Chemical and Biological Engineering, Environmental Inorganic Chemistry,
High Temperature Corrosion Center, Chalmers University of Technology, SE-41296 Göteborg, Sweden*

Polished 310 stainless steel coupons were exposed isothermally in a horizontal tube furnace at 500°C for 1–168 h. The exposure gas consisted of N_2 with 5% O_2 and 500 ppm HCl(g). The corroded samples were analyzed by X-ray diffraction, focused ion beam microanalysis, scanning electron microscopy with energy-dispersive X-ray analysis, and by Auger electron spectroscopy. Mass gain was recorded. As expected, HCl(g) is a corrosion accelerator, the dominating corrosion products being $FeCl_2$, Fe_2O_3, and Cr_2O_3. A tentative mechanism for the initial stages of the HCl-induced corrosion of stainless steel is presented.
© 2007 The Electrochemical Society. [DOI: 10.1149/1.2754174] All rights reserved.

It is well-known that hydrogen chloride is corrosive toward many metals and alloys at high temperature. Accordingly, the high corrosivity in boilers firing municipal waste is usually attributed (at least partly) to the appreciable HCl(g) levels (100–1000 ppm) in the flue gas. The alloys selected for use in HCl-containing environments are often chromia formers, including different types of stainless steel.

Numerous studies have investigated the corrosive effect of HCl(g) or Cl_2(g) on pure metals[1-5] and alloys.[6-17] The corrosive action of Cl-containing species at high temperature is usually explained within the framework of the so-called "active oxidation" mechanism in which Cl_2 and $MeCl_2$ molecules play a crucial role.[3,4,6,8] In this mechanism, Cl_2 is suggested to penetrate the protective oxide in gaseous form. When Cl_2 reaches the metal/oxide interface, the oxygen partial pressure is low and the formation of metal chlorides (such as $FeCl_2$) becomes thermodynamically favored. The metal chlorides are volatile and diffuse outward through the scale as gas molecules. The latter process has been suggested to be the rate-controlling step in the reaction mechanism.[3,8] When the metal chloride molecules reach the scale/gas interface, the environment is oxidizing, causing them to decompose into nonprotective porous metal oxide and Cl_2.[3,4] The released chlorine molecules then penetrates the oxide again, closing the "chlorine cycle." The process is believed to account for the porous and poorly adherent scale that often is formed in the presence of chlorine-containing species.[3,4]

An apparent problem with the "active oxidation" mechanism is the transportation of Cl_2(g) through the oxide. As noted above, elemental chlorine is supposed to form metal chlorides at the scale/metal interface where the oxygen activity is low. This implies that oxide is permeable to the Cl_2 molecule while being impermeable to the smaller O_2 molecule. Why does chlorine, but not oxygen, penetrate the oxide? Grabke[8] has suggested that chlorine creates fast diffusion paths in the oxide. However, regardless of how the pathways for Cl_2 molecular diffusion are created, they must also be fast diffusion paths for oxygen molecules, implying that the thermodynamic conditions for metal chloride formation are no longer fulfilled. The outward diffusion of gaseous metal chlorides has similar difficulties. Metal chloride molecules are much larger than Cl_2 or O_2 and cannot penetrate an oxide that prevents the diffusion of gaseous O_2. Another problem with active oxidation is that it predicts that chlorides are confined to the metal/scale interface. However, it has been reported[16] that chlorine-rich areas are also present in the outer part of the scale.

The present paper sets out to study initial stages of the HCl-induced corrosion of the chromia-forming AISI 310 stainless steel at 500°C using a combination of gravimetry and scale microstructure investigations. Scale cross sections prepared by focused ion beam (FIB) milling are investigated and the composition of the scale is studied by Auger electron spectroscopy (AES), energy-dispersive X-ray (EDX), and X-ray diffraction (XRD). It is shown that it is not necessary to postulate gas-phase transport of molecules through the scale in order to explain the HCl-induced corrosion of stainless steel.

Experimental

The alloy studied is AISI 310 stainless steel (see Table I for chemical composition). The geometrical area of the samples was 5.56 cm^2. A hole (ϕ = 1.5 mm) was drilled for handling. Before exposure the samples were ground to 1000 grit on SiC and polished with 1 μm diamond suspension until the surface appeared mirrorlike. The polished samples were degreased and cleaned in acetone and ethanol using ultrasonic agitation. The gravimetric measurements were made using a Sartorius balance with microgram resolution.

The exposures were performed in a horizontal silica tube furnace. The temperature was kept at 500 ± 1°C. The atmosphere consisted of N_2 with 5% O_2 and 500 ppm HCl (reference exposures without HCl were also carried out). HCl was added from a premixed 5% HCl–95% N_2 gas mixture using a digital mass flow regulator. The samples were mounted three at a time on an alumina sample holder. The samples were positioned parallel to the direction of the gas flow, in the center of the furnace. All parts of the system were kept >100°C to prevent the formation of aqueous surface films that would absorb HCl(g). The samples were stored in desiccators over P_2O_5 after exposure.

XRD.— A Siemens D5000 powder diffractometer with grazing-incidence geometry was used for XRD analysis. The instrument was equipped with a Göbel mirror. Cu Kα radiation with an angle of incidence varying between 0.3 and 1° was used. The measuring range was 10° < 2θ < 70°.

SEM and FIB.— Analytical electron microscopy was performed by a FEI Quanta ESEM 200 with a field emission gun. The microscope was operated in high-vacuum mode, and the samples were analyzed by both secondary and backscattered electrons. The instrument was equipped with an Oxford Inca EDX system. The acceleration voltage for imaging was between 8 and 12 kV. For EDX analysis the acceleration voltage varied between 5 and 30 kV. Cross sections of the corroded surfaces were prepared by a FEI Strata Dualbeam 235 FIB workstation. It is a FIB-SEM, with both an elec-

* Electrochemical Society Active Member.
[z] E-mail: nicklas.folkeson@chalmers.se

Table I. Chemical composition of AISI 310.

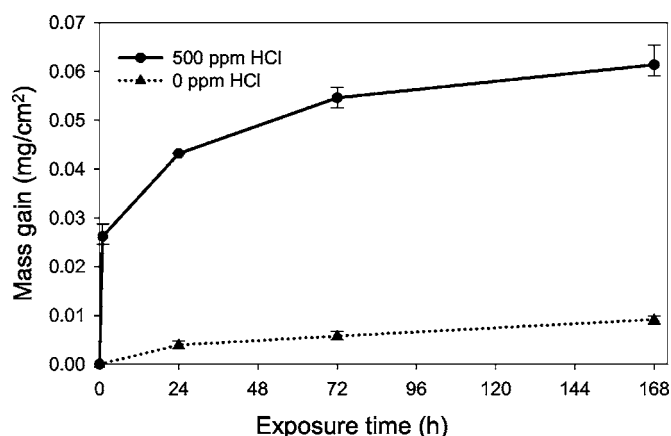| Element	Fe	Cr	Ni	Mn	Si	Mo	Cu	Co
Wt %	52.98	24.95	19.20	1.55	0.45	0.34	0.20	0.12
Atom %	52.15	26.38	17.98	1.55	0.88	0.19	0.17	0.11

Figure 1. Mass gain of alloy 310 in the presence and absence of 500 ppm HCl in 5% O_2 at 500°C.

tron column, equipped with FEG, and an ion column using a liquid Ga source. The instrument is also equipped with a gas injection system, enabling Pt deposition.

AES.— Measurements were conducted using a scanning Auger microprobe (PHI660), with an electron-beam voltage of 10 kV and current of about 160 nA. Depth profiles were obtained using a differentially pumped ion gun (Ar^+) with acceleration voltages between 1.5 and 4 kV. Multipak v6.0a software was used for raw data refining. The software enables evaluation of the peak shape of differentiated Auger peaks. This feature is useful for distinguishing between oxidized and metallic iron and chromium, as these elements have significant chemical shifts for the oxidized state.

Results

The corrosive effect of HCl(g) on alloy 310 is illustrated by the mass gain curve in Fig. 1. A comparison to the corresponding curve without added HCl shows that the effect of HCl(g) is practically instantaneous, a significant mass gain appearing already after 1 h. Subsequently, the curve levels off and assumes an approximately parabolic shape.

Figure 2 shows a SEM image and an AES depth profile of the oxide formed after 168 h in the absence of HCl. The oxide is thin (30–40 nm) and protective all over the surface, AES showing an enrichment of chromium near the alloy/oxide interface. The oxide formed over steel grain boundaries is clearly different from that on the steel grains. The XRD analysis showed only corundum-type oxide, $(Cr,Fe)_2O_3$.

The samples exposed to HCl can be described in terms of a few distinctive surface morphologies, namely, large corrosion product crusts and the rest of the scale, consisting of smooth and rough areas and ridges (compare Fig. 3 and 10). The corrosion product crusts are spatially separated, most of the surface being covered by the scale. XRD analysis of the samples exposed to HCl showed the presence of Fe_2O_3, Cr_2O_3, and iron(II) chloride. Figure 3 shows the scale after different exposure times in the presence of HCl. After 1 and 24 h the substrate grain structure is clearly visible, ridges having formed in the scale above the steel grain boundaries. The scale consists of alternating rough and smooth areas (appearing dark and bright in the SEM images, respectively), the morphology varying from substrate grain to substrate grain. The extent of the smooth scale diminishes with exposure time and it is completely replaced by rough scale after 168 h. Scattered flaky crystallites appear on the surface after 72 and 168 h. Figure 4 shows an AES depth profile of the smooth scale after 24 h. It consists primarily of an outer, chromium-rich part and an inner, iron-rich part. The chlorine is not confined to the metal/scale interface, chlorine levels of 5–9 atom % being present throughout the smooth scale. Figure 5 shows the cor-
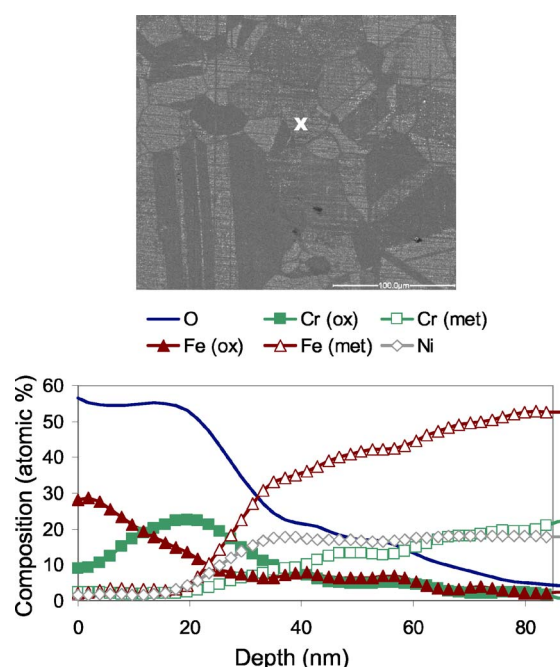

Figure 2. (Color online) SEM image and Auger depth profile after 24 h in 5% O_2 at 500°C in the absence of HCl.

responding AES depth profile of the rough scale after 24 h. A comparison with Fig. 4 shows that this part of the scale is thicker than the smooth scale and that it has a completely different composition. The outer part of the rough scale mainly consists of iron-rich oxide while the inner part is dominated by chromium-rich oxide. The rough scale contains much less chlorine (1–3 atom %); moreover, chlorine tends to be concentrated at the metal/scale interface.

The ridges that form in the scale over the steel grain boundaries are enriched in chlorine (see Fig. 6). After longer exposure time (24 h or more) nickel is enriched in the steel grain boundaries. After prolonged exposure the scale tends to crack and spall. Figure 7 shows the steel surface beneath a spalled part of the scale (after 72 h exposure). The steel grain boundaries are clearly visible, and also some darker, chlorine-rich features above the steel grain boundaries. From the EDX map it is not evident to which transition metal chlorine is associated, but XRD analysis confirmed the presence of $FeCl_2$ on all samples. Interestingly, nickel is not correlated to chlorine in these features.

Figure 8 shows a FIB cross section of the scale, showing two scale ridges that have formed over grain boundaries in the steel. EDX analysis revealed that the darker, inner part of the scale ridges contains metal chloride, while there is little chlorine at the scale/gas interface (the bright area directly beneath the platinum layer). Most of the scale ridges consist of metal chlorides. EDX analysis also showed that nickel is enriched in the steel grain boundaries beneath the metal/scale interface.

Metal chloride can be found on top of the scale on samples exposed for 72 h or longer. Figure 9 shows an EDX analysis of such a feature after 72 h exposure. The crystalline formations in the center of the image show up bright in the chlorine map. These formations lie on top of the scale. This is indicated by their sharpness and that they are dark in the oxygen map. The more diffuse and broader, chlorine-rich streaks surrounding these features correspond to metal chloride beneath the scale surface.

Figure 10 shows typical large corrosion crusts. With exposure time the crusts grow in size while the number density remains constant. After 1 h many tubular oxide whiskers protrude from the corrosion crust. As the corrosion crusts grow the whiskers become
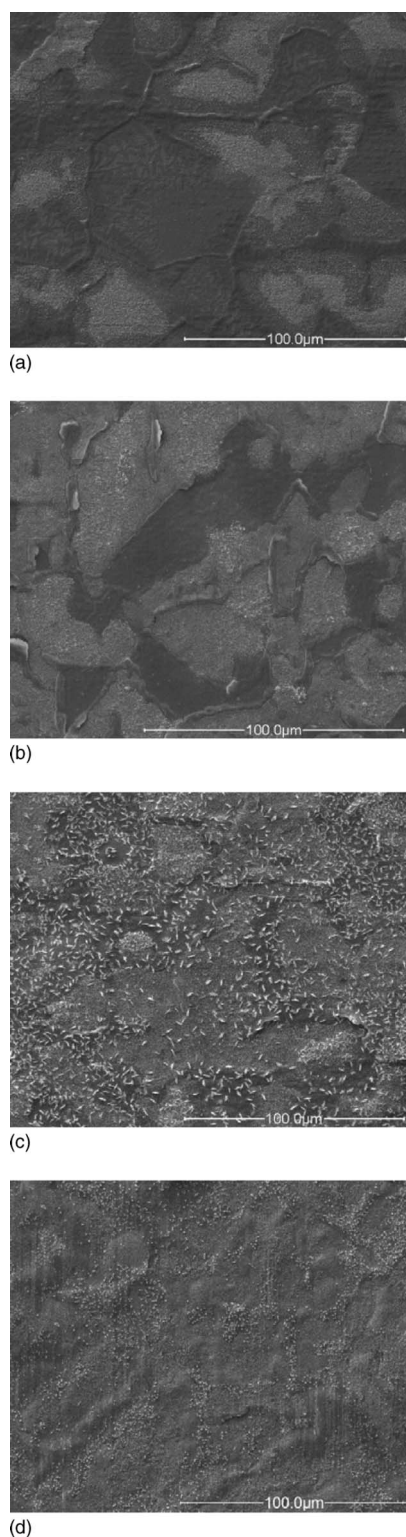
(a)

(b)

(c)

(d)

Figure 3. SEM images after (a) 1 h, (b) 24 h, (c) 72 h, and (d) 168 h exposure in 500 ppm HCl and 5% O_2 at 500°C.
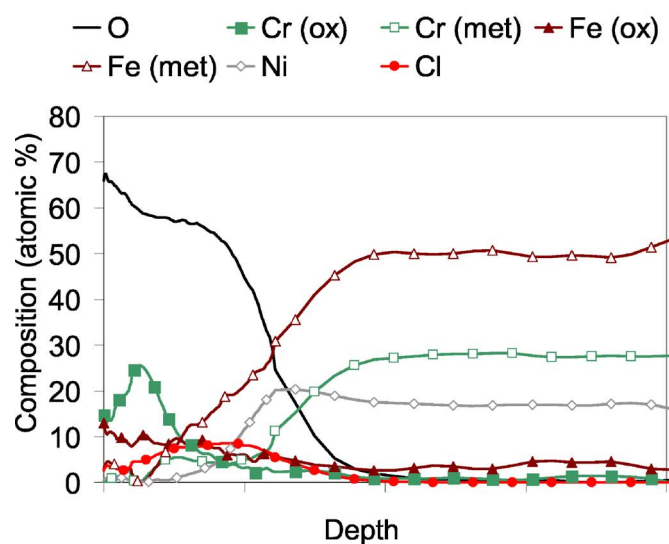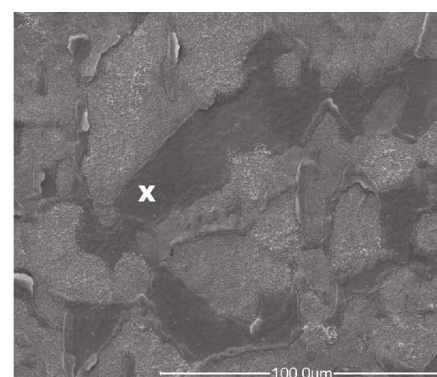

Figure 4. (Color online) SEM image and Auger depth profile of the smooth scale after 24 h in 500 ppm HCl and 5% O_2 at 500°C.
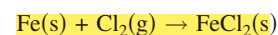
The lower part with the whiskers and the upper part with the thicker scale have high chlorine levels, and the chlorine is spreading laterally from the localized attack.

FIB cross sections through these corrosion crusts confirm that they form over slag inclusions in the steel surface (see Fig. 12). The corrosion crusts are very porous. Chlorine is not confined to the scale/metal interface, the entire corrosion crust containing chlorine. Chlorine concentrations reaching 40 atom % were detected at the scale/gas interface. Iron chlorides are also detected between the nonmetallic inclusion and the steel substrate.
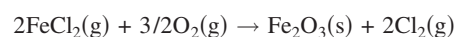
Discussion

This work confirms the corrosive nature of HCl(g), the addition of 500 ppm hydrogen chloride in O_2 resulting in a marked acceleration of the corrosion of the chromia-forming alloy 310 at 500°C. The prominent role played by metal chlorides in the corrosion process is in accordance with reports in the literature.[3,4,7,8,13,15,16]

In the "active oxidation" mechanism (see introduction) metal chlorides form at the scale/metal interface, according to Reaction 1, and diffuse to the scale/gas interface where they decompose, forming metal oxide and chlorine, see Reaction 2

$$Fe(s) + Cl_2(g) \rightarrow FeCl_2(s)$$

$$\Delta G°(500°C) = -243.45 \text{ kJ}^{18} \qquad [1]$$

$$2FeCl_2(g) + 3/2 O_2(g) \rightarrow Fe_2O_3(s) + 2Cl_2(g)$$

$$\Delta G°(500°C) = -256.70 \text{ kJ}^{18} \qquad [2]$$

more rare. The corrosion crusts are generally rounded, but after 168 h some of the largest corrosion crusts have toppled over.

Figure 11 shows an early stage in the formation of a corrosion crust. EDX analysis shows that the center of the "corrosion crust" is rich in calcium, silicon, and oxygen, corresponding to a nonmetallic inclusion (slag particle) in the steel. The corrosion crust has started to form above the inclusion, indicating a poorly protective oxide.
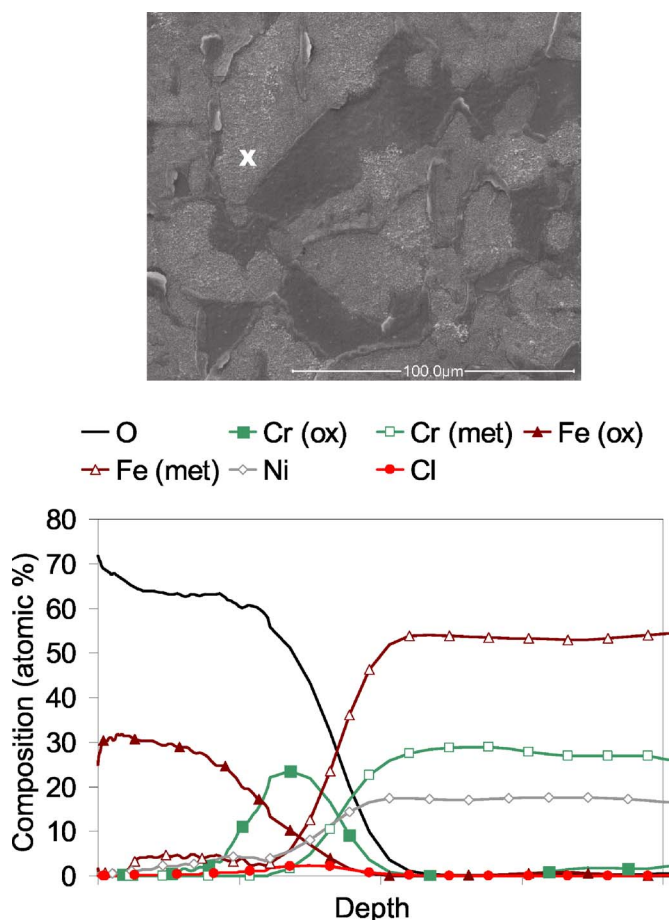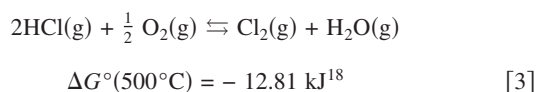
Figure 5. (Color online) SEM image and Auger depth profile of the rough scale after 24 h in 500 ppm HCl and 5% O_2 at 500°C.
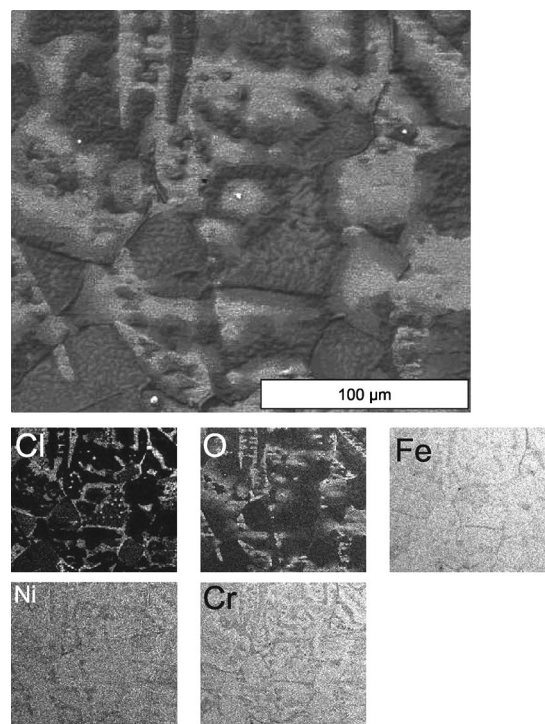

Figure 6. SEM image and elemental distribution after 1 h in 500 ppm HCl and 5% O_2 at 500°C.

$\times\ 10^{-6}$ bar.[18] The Cl_2 molecule dissociates easily and is a powerful oxidant. It is suggested that it is reduced at the scale surface, forming chloride ions, the necessary electronic current being provided by metal oxidation at the scale/metal interface
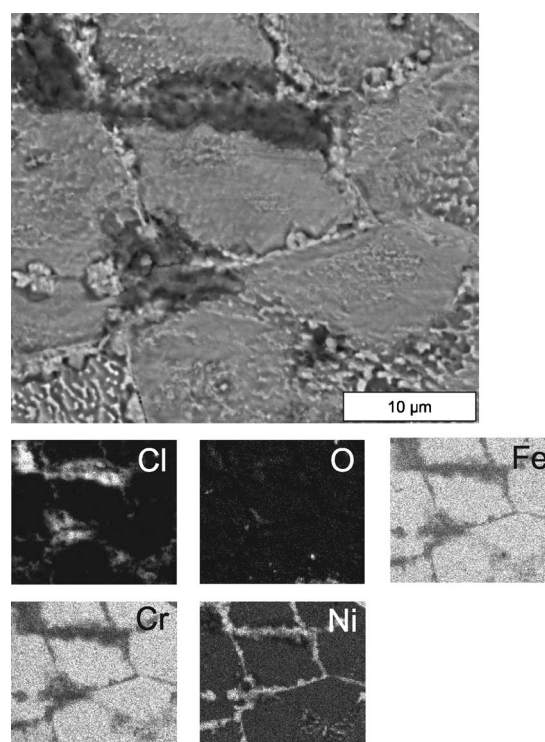
Because of the gradient in oxygen activity through the scale, the metal chlorides are confined to the metal/oxide interface. As we move away from it, the environment becomes more oxidizing and consequently, the metal chlorides are expected to be converted to metal oxide. However, the present results are clearly not in line with these predictions. On the contrary, the results show that metal chloride is distributed throughout the thickness of the smooth scale (Fig. 4). This is in agreement with Zahs et al., who report that iron chloride, formed on pure iron in the presence of HCl, is not confined to the scale/metal interface.[16] Moreover, the present study shows that solid iron chloride is present even at the scale/gas interface.

Hence, it appears that the observations in the present study cannot be explained by the "active oxidation" mechanism. Instead, an alternative approach is proposed that does not involve gas-phase transport through the scale. In the new reaction scheme, the reduction reaction at the scale surface and the oxidation of metal at the scale/metal interface are coupled by the migration of anions and cations and by an electronic current. The reaction scheme mainly applies to early stages of corrosion attack, corresponding to the rapid initial mass gain and the smooth scale and the ridges in the scale. Let us first consider the oxidation of HCl by O_2 in the gas phase (the Deacon process)

$$2HCl(g) + \tfrac{1}{2}\,O_2(g) \leftrightarrows Cl_2(g) + H_2O(g)$$

$$\Delta G°(500°C) = -12.81\ kJ^{18} \qquad [3]$$

Thermodynamic equilibrium under our experimental conditions (with input gas composition = 5% O_2, 10 ppm H_2O, and 500 ppm HCl at 1 bar and 500°C) corresponds to $PCl_{2(eq)}$ = 150

Figure 7. SEM image and elemental distribution from a part of the surface where the scale has spalled (72 h in 500 ppm HCl and 5% O_2 at 500°C).
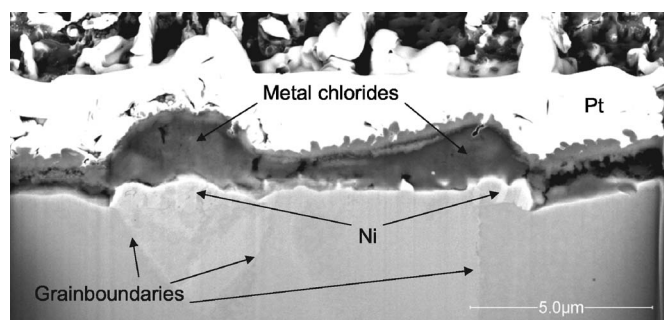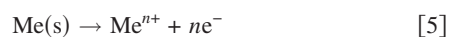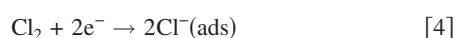
Figure 8. FIB cross section of the scale after 72 h in 500 ppm HCl and 5% O_2 at 500°C. The cross section was made at 52° tilt.

$$Cl_2 + 2e^- \rightarrow 2Cl^-(ads) \qquad [4]$$

$$Me(s) \rightarrow Me^{n+} + ne^- \qquad [5]$$

The formation of elemental chlorine by Reaction 3 is slow at 500°C in the absence of a catalyst[19] and it may be questionable whether the concentration of Cl_2 at the scale surface is high enough to explain the rapid initial uptake of chlorine by the sample. However, chloride ions can also be generated on the surface without involving the chlorine molecule
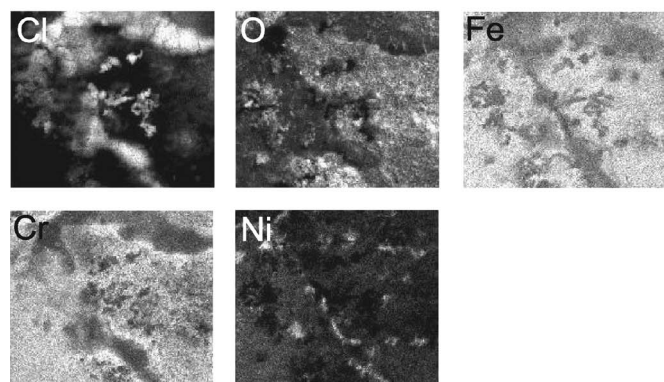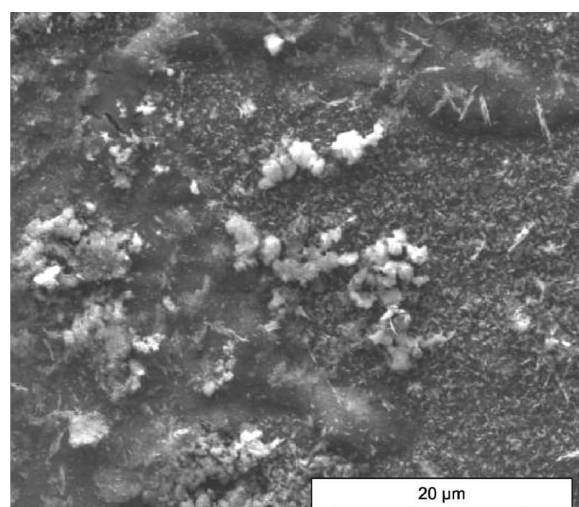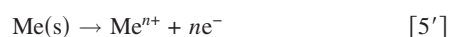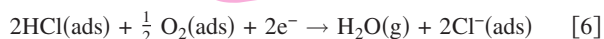
$$2HCl(ads) + \tfrac{1}{2} O_2(ads) + 2e^- \rightarrow H_2O(g) + 2Cl^-(ads) \qquad [6]$$

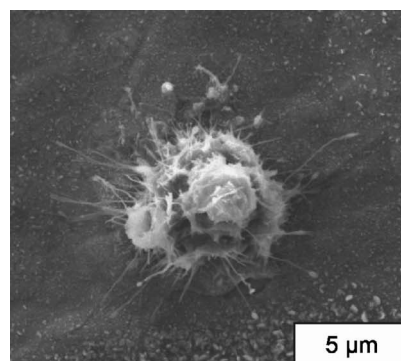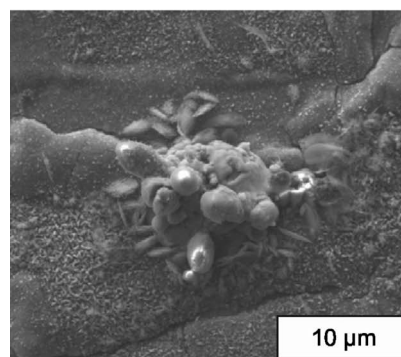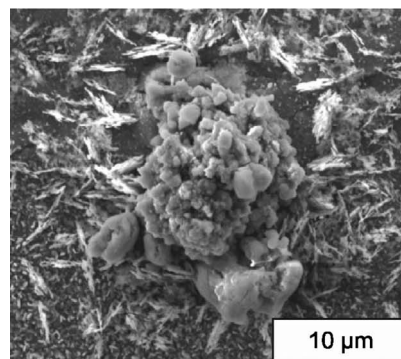$$Me(s) \rightarrow Me^{n+} + ne^- \qquad [5']$$

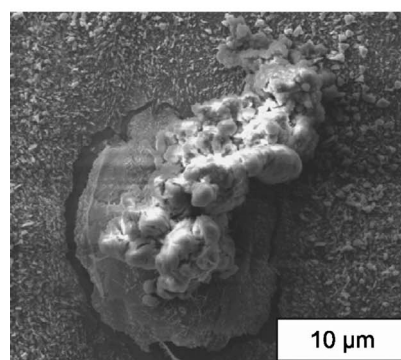**Figure 9.** Metal chloride particles on the scale surface of a sample exposed to 500 ppm HCl and 5% O_2 at 500°C for 72 h.

Figure 10. SEM images of localized attack on samples exposed to 500 ppm HCl and 5% O_2 at 500°C, after (a) 1 h, (b) 24 h, (c) 72 h, and (d) 168 h.

In this case the cathodic current is provided by oxygen reduction rather than chlorine reduction. Simultaneously, adsorbed HCl is deprotonated, forming water. Chloride is not expected to substitute for oxide ions in an ionic oxide because of its large size and small
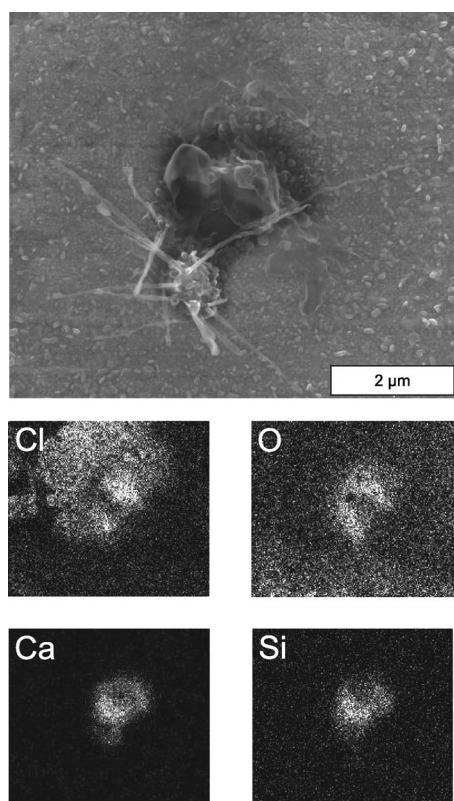
Figure 11. SEM image of the initial stages of a localized attack. Sample exposed to 500 ppm HCl and 5% O_2 at 500°C for 1 h.

Figure 12. FIB cross section of a corrosion product crust after 24 h in 500 ppm HCl and 5% O_2 at 500°C. The cross section was made at 52° tilt. Investigations by EDX showed that chromium is the dominant cation in the oxide part of the crust.

charge. This is in accordance with the lack of evidence for chloride dissolution in magnetite and hematite. However, the same restrictions do not apply to the oxide surface where chloride ions can freely adsorb. Surface chloride is expected to have higher mobility than surface oxide ions because of the smaller charge/radius ratio. Grain boundaries in a polycrystalline material can be regarded as "inner surfaces" and have properties similar to those of a free surface.[20] This explains the characteristically low activation barriers for diffusion and correspondingly high diffusivities in grain boundaries, e.g., in protective oxides. Hence, it is proposed that in the present case, the anionic current is to a large extent carried by chloride ions that penetrate the scale by grain boundary diffusion.

The EDX and XRD results imply that chloride is associated with iron in the form of $FeCl_2$. It is assumed that iron chloride forms as a result of the combination of chloride ions and ferrous ions. Hence, the occurrence of iron chloride throughout the thickness of the smooth scale (Fig. 5) and at the scale/gas interface (Fig. 9) implies that outward Fe^{2+} migration has occurred, the location of iron chloride formation depending on the relative speed of outward Fe^{2+} migration and inward Cl^- migration. The iron chloride in the scale is expected to be a much better conductor of ions than the oxide. Hence, the flow of ions through the scale (and the corrosion rate) increases as more and more iron chloride accumulates. The accumulation of iron chloride at the scale/metal interface is also expected to decrease scale adhesion. In accordance, Fig. 7 shows extensive cracking and spallation of the scale after 72 h in the presence of HCl.

The occurrence of iron chloride on the scale surface (Fig. 9) may seem surprising because the formation of $FeCl_2$ from hematite and HCl (Reaction 7) is thermodynamically disallowed in our experimental conditions (500 ppm HCl, 5% O_2, 500°C). It is argued that the formation of $FeCl_2$ at the scale surface is made possible in the present case by the corroding metal below the scale, the anodic
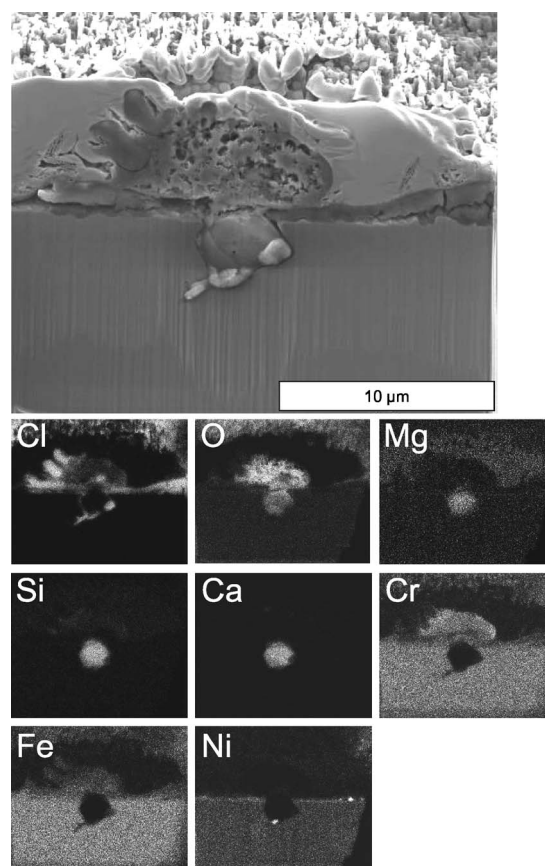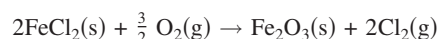
reaction providing the necessary electrons for chloride ions to form on the surface (see Reactions 4-6). On the scale surface, $FeCl_2$ tends to decompose, leaving a hematite residue

$$2FeCl_2(s) + \tfrac{3}{2} O_2(g) \rightarrow Fe_2O_3(s) + 2Cl_2(g)$$

$$\Delta G°(500°C) = -129.00 \text{ kJ}^{18} \qquad [7]$$

The presence of significant amounts of metastable iron chloride on the sample surface after exposure shows that its decomposition is comparatively slow. As mentioned above, ferrous chloride is thermodynamically stable at the scale metal interface. The equilibrium vapor pressure of $FeCl_2(g)$ over $FeCl_2(s)$ at 500°C is 3×10^{-5} bar,[18] implying that vaporization must be taken into account and that mass gain is not necessarily a good measure of corrosion rate when iron chloride is formed.

In addition to iron chloride, the smooth scale mainly consists of chromium oxide (see Fig. 4). It is suggested that the predominance of chromium oxide over iron oxide is due to its thermodynamic stability. In analogy to iron ions, chromium ions are expected to combine with chloride ions, forming $CrCl_2$ or $CrCl_3$. It is suggested that the absence of chromium chloride in the thin scale and scale ridges is due to the spontaneous reaction between chromium chloride and hematite, forming chromium(III) oxide

$$2CrCl_2(s) + Fe_2O_3(s) \rightarrow 2FeCl_2(s) + Cr_2O_3(s)$$
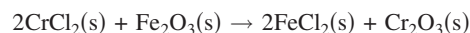
$$\Delta G°(500°C) = -203.10 \text{ kJ}^{18} \qquad [8]$$

The composition of the ridges in the scale that form over steel grain boundaries is similar to that of the thin scale ($FeCl_2$ + Cr_2O_3). The more rapid growth of the scale in this case is attrib-

uted to impurities in the initial oxide, making it more vulnerable to HCl attack. With time the smooth $FeCl_2 + Cr_2O_3$ scale is replaced by a rough scale that contains much less chloride. The bottom part of the rough scale is enriched in chromium oxide, suggesting that it is protective. This morphology corresponds to a partial decomposition and/or vaporization of the iron chloride in the smooth scale formed initially.

The localized attack associated with the slag inclusions shows similarities to the smooth scale and the scale ridges, the main corrosion products being $FeCl_2$ and Cr_2O_3 (see Fig. 11 and 12). It is suggested this type of corrosion occurs by a similar mechanism as described for the initial stages of rapid metal chloride formation. It appears that the presence of a slag inclusion at the steel surface makes it extremely susceptible to this type of attack. It is argued that the oxide is less protective above impurities and faults in the steel surface, causing increased ion transport and consequently, localized attack. As shown in Fig. 11, chlorine spreads laterally from the localized attack at slag inclusions and may thus enhance the general corrosion.

Conclusions

HCl accelerates the corrosion of alloy 310 in dry O_2 at 500°C. Initially a smooth scale forms, mainly consisting of Cr_2O_3 and $FeCl_2$. Iron chloride is present throughout the scale and also at the scale/gas interface. $FeCl_2$-rich ridges form in the scale over steel grain boundaries. Rapid localized corrosion is observed at slag inclusions in the alloy surface, forming mainly Cr_2O_3 and $FeCl_2$. A reaction scheme is presented for the initial stages of corrosion. In the scheme, the formation of chloride ions on the scale surface is coupled to metal oxidation at the scale/metal interface by electronic current and by the grain boundary migration of chloride ions and cations. In contrast to active oxidation, the present reaction scheme

does not involve the diffusion of Cl_2 or metal chloride molecules through the scale. With time a rough scale forms that mainly consists of $(FeCr)_2O_3$ oxide. This is explained by the decomposition and vaporization of $FeCl_2$.

References

1. S. Y. Lee and M. J. McNallan, *J. Electrochem. Soc.*, **137**, 472 (1990).
2. S. Y. Lee and M. J. McNallan, *Corrosion (Houston)*, **47**, 868 (1991).
3. Y. Y. Lee and M. J. McNallan, *Metall. Trans. A*, **18**, 1099 (1987).
4. M. J. McNallan, W. W. Liang, S. H. Kim, and C. T. Kang, *High Temperature Corrosion*, p. 316, NACE, Houston, TX (1983).
5. F. H. Stott and C. Y. Shih, *Mater. Corros.*, **51**, 277 (2000).
6. J.-M. Abels and H.-H. Strehblow, *Corros. Sci.*, **39**, 115 (1997).
7. R. Bender and M. Schutze, *Mater. Corros.*, **54**, 652 (2003).
8. H. J. Grabke, E. Reese, and M. Spiegel, *Corros. Sci.*, **37**, 1023 (1995).
9. V. A. C. Haanappel, N. W. J. Haanappel, T. Fransen, H. D. van Corbach, and P. J. Gellings, *Corrosion (Houston)*, **48**, 812 (1992).
10. A. S. Kim and M. J. McNallan, *Corrosion (Houston)*, **46**, 746 (1990).
11. J. C. Liu and M. J. McNallan, *Mater. Corros.*, **50**, 253 (1999).
12. S. Sroda, S. Tuurna, K. Penttila, and L. Heikinheimo, *Mater. Sci. Forum*, **461–464**, 981 (2004).
13. F. H. Stott and C. Y. Shih, *Oxid. Met.*, **54**, 425 (2000).
14. N. Sämann, M. Spiegel, and H. J. Grabke, *Mater. Sci. Forum*, **369–3**, 963 (2001).
15. A. Zahs, M. Spiegel, and H. J. Grabke, *Mater. Corros.*, **50**, 561 (1999).
16. A. Zahs, M. Spiegel, and H. J. Grabke, *Corros. Sci.*, **42**, 1093 (2000).
17. X. J. Zheng and R. A. Rapp, *Oxid. Met.*, **48**, 553 (1997).
18. I. Barin, *Thermodynamic Data of Pure Substances*, VCH Verlagsgesellschaft mbH, Weinheim (1995).
19. K. Liu, W. P. Pan, and J. T. Riley, *Fuel*, **79**, 1115 (2000).
20. A. P. Sutton and R. W. Balluffi, *Interfaces in Crystalline Materials*, Oxford Science Publications, Oxford (1995).